Article

INTERNATIONAL JOURNAL OF DAMAGE MECHANICS

International Journal of Damage Mechanics
2014, Vol 23(1) 25–42

DOI: 10.1177/1056789513482599
ijd.sagepub.com

SAGE

Overall mechanical behavior of nanocrystalline materials accompanied by damage evolution on grain boundaries

Li Chen and Yueguang Wei

Abstract

In the present research, overall mechanical behaviors of the nanocrystalline materials considering the grain boundary damage evolutions are investigated systematically. A mixed-mode cohesive interface model is used to describe the mixed deformation and fracture process of grain boundaries. Based on the mixed-mode cohesive interface model, the grain boundary damage and damage evolution are defined and characterized. In order to describe the size effect, the strain gradient plasticity theory is used for grain materials. In the present results, the overall stress–strain relations and the corresponding damage evolution curves are obtained as functions of several independent parameters, such as the mixed separation strength, the mixed critical energy release rate, grain size, Young's modulus as well as strain hardening exponent. The present results show that both the overall strength and ductility of the nanocrystalline materials are closely dependent on the grain boundary strength and the damage evolution behaviors. By means of the damage evolution relations, the features of the overall stress–strain curves can be clearly interpreted.

Keywords

Grain boundary, damage evolution, fracture, nanocrystalline metals, mixed-mode cohesive model, finite element method

Introduction

Mechanical behaviors of polycrystalline materials with grain sizes typically at nano- or micron scale (such as nanocrystalline (NC) materials) have been attracting a great deal of interest over the past two decades. The NC metals exhibit higher yield strength, tensile strength and hardness, but lower tensile ductility relative to their bulk counterparts. In the previous investigations, several

State Key Laboratory of Nonlinear Mechanics, Institute of Mechanics, Chinese Academy of Sciences, Beijing, PR China

Corresponding author:

Li Chen, State Key Laboratory of Nonlinear Mechanics, Institute of Mechanics, Chinese Academy of Sciences, Beijing 100190, PR China.

Email: cchenli@Lnm.imech.ac.cn

mechanisms have been presented for governing the mechanical behaviors of polycrystalline aggregates (Gleiter, 2000; Kumar et al., 2003; Wei et al., 2005), very few direct experimental evidences reported about the fracture and failure processes for the NC metals, especially on the inelastic deformation competition between grain interior and grain boundary. Shan et al. (2004) have reported that the grain boundary-mediated process of the NC nickel film dominates its deformation in the observation using the transmission electron microscope (TEM). Moreover, the molecular dynamics (MD) simulations have shown that grain boundary-related slip and separation phenomena play an important role in the overall inelastic response with decreasing grain size (Cao and Wei, 2007; Hasnaoui et al., 2003; Schiotz et al., 1999; Van Swygenhoven and Derlet, 2001; Van Vliet et al., 2003). Due to the limitations of both time scale and dimension scale in MD simulations for the mechanical behaviors of the NC metals with realistic experiment sample sizes and strain rates, several continuum models have been used to describe the grain boundary effect and the failure response for the NC materials (Fu et al., 2004; Ovid'ko, 2007; Schwaiger et al., 2003; Warner et al., 2006; Wei and Anand, 2004; Wei et al., 2005, 2006). Considering the inherent characteristics of grain boundaries in the NC metals, both the grain boundary affected zone (GBAZ) model (Fu et al., 2004; Schwaiger et al., 2003; Wei et al., 2005, 2006) and the cohesive interface model (Warner et al., 2006; Wei and Anand, 2004; Wu and Wei, 2010; Wu et al., 2012) have been proposed to characterize the grain boundary response in polycrystalline aggregates. Especially, the cohesive interface model is used to describe both the interface strength and the interface damage evolution (Mi et al., 1998). Cohesive interface models are being increasingly used to describe damage and failure behaviors in a number of material systems (Nilsson and Lidstrom, 2012; Omiya and Kishimoto, 2010; Truong and Kitamura, 2010).

Specifically, Wu and Wei (2010) recently have studied the size effects of mechanical behavior for the NC metals by adopting both the cohesive interface model and the conventional theory of mechanism-based strain gradient plasticity (CMSG) (Huang et al., 2004). They used a normal separation cohesive model to describe the grain boundary separation in mode I. More recently, Wu et al. (2012) have presented a trans-scale mechanics theory with respect to both the interface energy effect and the strain gradient effect, and they have also used the normal separation cohesive model to describe the grain boundary fracture process.

Although the comprehensive analyses of mechanical behaviors for the NC materials by using above-mentioned continuum models were carried out recently, it is still difficult to unambiguously define the interfacial properties of grain boundaries. The conventional elastic–plastic theory also failed to characterize the size effects of intragranular deformation at nanoscale. Therefore, in the present research, overall mechanical behaviors of the NC metals accompanied by the grain boundary damage evolution are systematically investigated. We shall pay our attention to using a mixed-mode cohesive interface model to describe the grain boundary mixed deformation, separation as well as the fracture. In addition, the CMSG model (Huang et al., 2004) is used to characterize the strain hardening of grain materials at the small scale.

Problem formulations

Description for grain material

When grain size is at micro- or nanoscale, the mechanical behavior of the grain material cannot be well described by using the classical elastic–plastic theory. So, in the present research, a strain gradient theory is used. For simplifying the analysis, the CMSG theory (Huang et al., 2004) will be used. Unlike the general strain gradient plasticity theory (Gao et al., 1999; Wei and Hutchinson, 1997a), the CMSG

theory is a lower order theory which does not involve the higher order stress. Although it can only provide an approximate description for the problem (Evans and Hutchinson, 2009), it can easily develop a finite element scheme for describing size effect.

Briefly, the constitutive relation for CMSG (Huang et al., 2004) can be expressed as follows:

$$\dot{\sigma}_{ij} = K\dot{\varepsilon}_{kk}\delta_{ij} + 2\mu\left\{\dot{\varepsilon}'_{ij} - \frac{3\dot{\varepsilon}}{2\sigma_{\mathrm{e}}}\left(\frac{\sigma_{\mathrm{e}}}{\sigma_{\mathrm{Y}}\sqrt{f^2(\varepsilon^{\mathrm{p}}) + l\eta^{\mathrm{p}}}}\right)^m \sigma'_{ij}\right\} \tag{1}$$

where K is the bulk modulus, μ is the shear modulus, m is the rate-sensitivity exponent ($m \geq 20$) (Hutchinson, 1976; Kok et al., 2002) and ε^{p} and η^{p} are the effective plastic strain and plastic strain gradient, which can be expressed as

$$\eta^{\mathrm{p}} = \sqrt{\frac{1}{4}\eta^{\mathrm{p}}_{ijk}\eta^{\mathrm{p}}_{ijk}}, \quad \eta^{\mathrm{p}}_{ijk} = \varepsilon^{\mathrm{p}}_{ik,j} + \varepsilon^{\mathrm{p}}_{jk,i} - \varepsilon^{\mathrm{p}}_{ij,k}, \quad \varepsilon^{\mathrm{p}}_{ij} = \int \dot{\varepsilon}^{\mathrm{p}}_{ij}\mathrm{d}t, \quad \varepsilon^{\mathrm{p}} = \sqrt{2/3\varepsilon^{\mathrm{p}}_{ij}\varepsilon^{\mathrm{p}}_{ij}} \tag{2}$$

where l is the intrinsic material length scale in strain gradient plasticity, σ_{Y} is the initial yield stress, f is a non-dimensional function of plastic strain which for a power-law hardening solid takes the form as follows:

$$f(\varepsilon^{\mathrm{p}}) = \left(1 + \frac{E\varepsilon^{\mathrm{p}}}{\sigma_{\mathrm{Y}}}\right)^N \tag{3}$$

where E is the Young's modulus, N is the strain hardening exponent ($0 \leq N < 1$). $\dot{\varepsilon} = \sqrt{2/3\dot{\varepsilon}'_{ij}\dot{\varepsilon}'_{ij}}$ is the effective strain rate, $\dot{\varepsilon}'_{ij}$ is the deviatoric strain rate and $\sigma_{\mathrm{e}} = \sqrt{3\sigma'_{ij}\sigma'_{ij}/2}$ is the von Mises effective stress.

Grain boundary description

Grain boundary fracture process is described by using the cohesive interface model presented earlier by Barenblatt (1959, 1962) and Dugdale (1960). In past few decades, the cohesive interface model has undergone great improvements and developments in describing the material fracture process for the sake of the development of the finite element methods (FEMs; Needleman, 1990; Tvergaard and Hutchinson, 1992; Wei and Hutchinson, 1997b). The traction–separation (T–S) relations of cohesive interface model have been extended to represent the grain boundary fracture process (Warner et al., 2006; Wei and Anand, 2004; Xu et al., 2010). In the present investigation, a mixed-mode cohesive interface model developed by Turon et al. (2004) will be used to describe the grain boundary fracture process accompanied by the damage initiation and evolution.

Mixed-mode cohesive interface model. In the cohesive interface model, both height of area and area below the T–S relation stand for the interface separation strength and the interface energy release rate, respectively. As it is well known that keeping both height of area and area unchanged, the influence of changing shape of area on the modeling results for mechanical behaviors is small and can be neglected. Therefore, for simplification of analysis, in the present study, we shall use a bilinear mixed-mode cohesive model, which is shown in Figure 1(a) in a 3D map. Three coordinate axes are the normal relative displacement δ_{n}, shearing relative displacement δ_{s} and traction, respectively. As shown in Figure 1(a), both the triangles $\mathrm{O} - \mathrm{T}_{\mathrm{l}} - \delta^{\mathrm{f}}_{\mathrm{n}}$ and $\mathrm{O} - \mathrm{T}_{\mathrm{S}} - \delta^{\mathrm{f}}_{\mathrm{s}}$ (O is the origin of

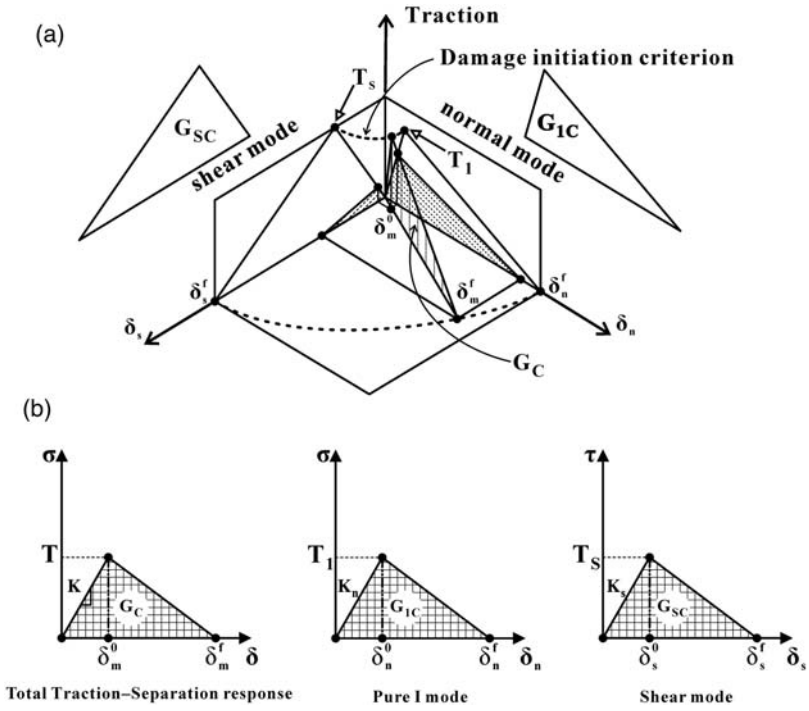

Figure 1. (a) Illustration of mixed-mode cohesive interface model and (b) bilinear T–S response.

coordinate) are the bilinear responses in pure normal and pure shear modes, respectively. Point located on the $O - \delta_s^f - \delta_n^f$ plane will correspond to a mixed-mode interface separation process state. Subscripts ''n'' and ''s'' are used to represent the pure separation mode and pure shear mode, respectively.

The critical relative displacements corresponding to the peak stress points are identified with the superscript ''0''. The limit relative displacements corresponding to failure state are identified with the superscript ''f''.

The relations between critical relative displacements and maximum tractions are given by

$$\delta_n^0 = \frac{T_1}{K_n}, \quad \delta_s^0 = \frac{T_S}{K_S} \tag{4}$$

where T_1 and T_S are the peak stresses, the limit tractions for pure separation mode and pure shear mode, respectively. K_n and K_s are the penalty stiffness.

The relations between the maximum relative displacements and fracture energies can be written as follows

$$\delta_n^f = \frac{2G_{1C}}{K_n \delta_n^0}, \quad \delta_s^f = \frac{2G_{SC}}{K_S \delta_s^0} \tag{5}$$

where G_{1C} and G_{SC} are the fracture energies for pure separation mode and pure shear mode, respectively.

In order to describe the combined effect of normal and shear deformations across the interface, an effective relative displacement is defined as follows

$$\delta_{\mathrm{m}} = \sqrt{\langle \delta_{\mathrm{n}} \rangle^2 + \delta_{\mathrm{s}}^2} \tag{6}$$

where symbol $\langle \delta_{\mathrm{n}} \rangle$ is Macaulay bracket for δ_{n}, which signifies that its value is equal to zero for $\delta_{\mathrm{n}} < 0$, otherwise equal to δ_{n}, where δ_{n} and δ_{s} are the normal and tangential displacements along the interface, respectively.

The mixed-mode T–S relations are illustrated in Figure 1(b), where σ is the traction, δ_{m}^0 is the critical separation displacement at the peak stress, T is the critical traction and $\delta_{\mathrm{m}}^{\mathrm{f}}$ is limit separation displacement. Both δ_{m}^0 and $\delta_{\mathrm{m}}^{\mathrm{f}}$ can be determined by using the mixed-mode strength and fracture criteria according to the following equations (7) and (8), respectively.

The critical strength (damage initiation) condition is assumed when the following quadratic relation is satisfied (Mi et al., 1998):

$$\left(\frac{\langle \sigma_{\mathrm{n}} \rangle}{\mathrm{T_1}}\right)^2 + \left(\frac{\tau_{\mathrm{s}}}{\mathrm{T_S}}\right)^2 = 1 \tag{7}$$

where σ_{n} and τ_{s} are the normal and shear stresses on the interface, respectively. $\mathrm{T_1}$ and $\mathrm{T_S}$ are the limit separation and shear tractions, respectively.

The mixed-mode fracture criterion is described as follows (Mi et al., 1998):

$$\frac{\mathrm{G_1}}{\mathrm{G_{1C}}} + \frac{\mathrm{G_S}}{\mathrm{G_{SC}}} = 1 \tag{8}$$

where $\mathrm{G_1}$ and $\mathrm{G_S}$ are the current fracture energies for the normal and shear components, respectively, $\mathrm{G_C} = \mathrm{G_1} + \mathrm{G_S}$ is the total current fracture energy for mixed-mode case when above condition is satisfied.

Damage evolutions on grain boundary. The cohesive interface model is used to describe the interface mechanical properties by adopting the two major parameters, such as the separation strength (height) and the energy release rate (area). On the other hand, the cohesive interface model can be taken as an interface damage model, taking the bilinear model as the example (Figure 1b): at the first stage, the interface separation under the action of traction is according to a linear-elastic law, then when relative separation displacement obtains a critical value δ_{m}^0, damage occurs and evolves with further increasing the relative separation displacement along soft straight line.

In order to characterize the grain boundary damage evolution, it is convenient to define a damage variable D. Its definition can be described as a ratio of ''nominal dissipation energy'' to ''nominal total energy''. As shown in Figure 2, assuming that the cohesive state is currently at the Point B, the nominal total energy can be expressed as the triangular area OCE (area S) without considering the damage, and the nominal dissipation energy can be calculated as the triangular area OBE (area $\mathrm{S_1}$), so that the damage variable D is equal to an area ratio $\mathrm{S_1/S}$. One can easily derive out as follows (Turon et al., 2004),

$$\mathrm{D} = \begin{cases} 0, & \delta_{\mathrm{m}} \le \delta_{\mathrm{m}}^0 \\ \dfrac{\delta_{\mathrm{m}}^{\mathrm{f}}\left(\delta_{\mathrm{m}} - \delta_{\mathrm{m}}^0\right)}{\delta_{\mathrm{m}}\left(\delta_{\mathrm{m}}^{\mathrm{f}} - \delta_{\mathrm{m}}^0\right)}, & \delta_{\mathrm{m}}^0 < \delta_{\mathrm{m}} \le \delta_{\mathrm{m}}^{\mathrm{f}} \\ 1, & \delta_{\mathrm{m}} \ge \delta_{\mathrm{m}}^{\mathrm{f}} \end{cases} \tag{9}$$

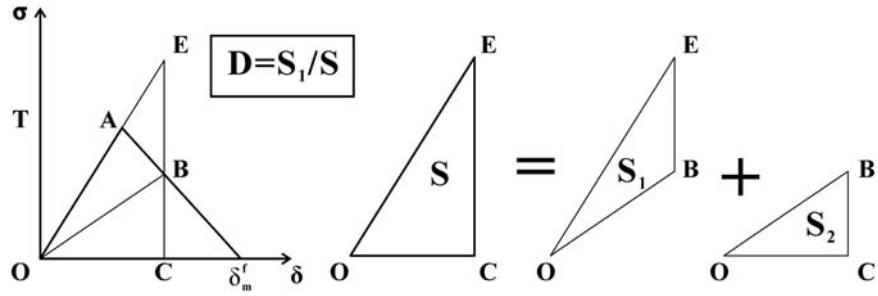

Figure 2. Damage definition based on the cohesive interface model.

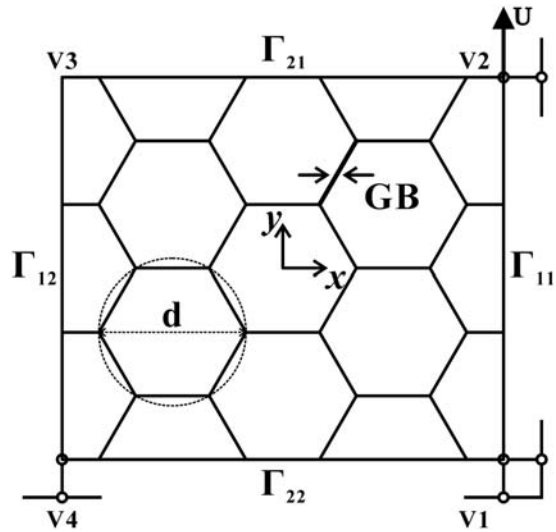

Figure 3. A representative cell model for nanocrystalline metal with periodic boundary conditions of *xy* plane and *z* direction.

where δ_m^0 and δ_m^f are the critical relative displacement corresponding to the peak stress point and the limit relative displacement, respectively, which can be attained by using the mixed-mode strength and fracture criteria (see equations (7) and (8), respectively).

Numerical simulations

Cell model and periodic boundary conditions

A regular quasi-three-dimensional cell model is presented here. Figure 3 shows the schematic drawing of the cell model. The cell model is consisted of 12 regular hexagon grains, and the grain size d is the diameter of the circum circle of regular hexagon. The separation and damage evolution process of grain boundary between any two hexagon grains is modeled by using a single layer of the cohesive elements with zero thickness, as shown in Figure 3.

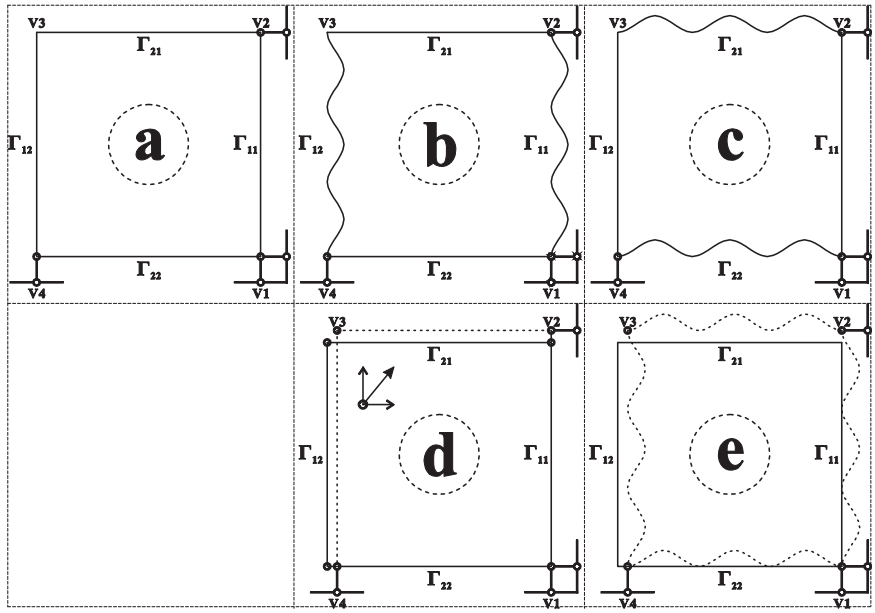

Figure 4. Illustration of periodic boundary conditions.

For NC materials considered in the present research, the periodic boundary conditions are applied. As shown in Figure 3, periodic boundary conditions are enforced along the four sides in *xy* coordinate plane (Van der Sluis et al., 2001):

$$\vec{\mathbf{u}}_{12} - \vec{\mathbf{u}}_{V4} = \vec{\mathbf{u}}_{11} - \vec{\mathbf{u}}_{V1} \tag{10}$$

$$\vec{\mathbf{u}}_{22} - \vec{\mathbf{u}}_{V1} = \vec{\mathbf{u}}_{21} - \vec{\mathbf{u}}_{V2} \tag{11}$$

$$\vec{\mathbf{u}}_{V3} - \vec{\mathbf{u}}_{V2} = \vec{\mathbf{u}}_{V4} - \vec{\mathbf{u}}_{V1} \tag{12}$$

Here, $\vec{\mathbf{u}}_{ij}$ is a displacement vector for a material point on the boundary Γ_{ij}, and $\vec{\mathbf{u}}_{Vi}$ is a displacement vector for the vertex Vi. Rigid displacements can be eliminated by requiring $\vec{\mathbf{u}}_{Vk} = 0$, for either $k \in \{1,2,4\}$.

In order to display the three-dimensional effect, a displacement vector $\vec{\mathbf{u}}_z$ on boundary is enforced in the *z* coordinate direction, assuming that the material geometry in *z* direction is also a periodic structure which has a finite thickness.

An arbitrary periodically deformed unit cell under uniaxial tensile condition is shown in Figure 4, where (a) represents the initial undeformed state. The deformed states of equations (10)–(12) correspond to the cases of (b)–(d) in Figure 4, respectively. Figure 4(e) represents the deformed state under periodic boundary conditions.

Descriptions of overall mechanical behavior and damage evolution

The main purpose of the present research is not only to simulate the overall mechanical behavior, but also to provide some insights into the damage evolution when the NC material underwent the

periodic loading. A systematical parametric study is performed. The overall stress–strain relation normalized by the initial yield stress σ_Y and the intrinsic material length l with parameter dependence can be expressed as

$$\frac{\sigma}{\sigma_Y} = f\left(\varepsilon;\ \underbrace{\frac{E}{\sigma_Y},\ \ v,\ \ N,\ \ \frac{d}{l}}_{\text{intragranular parameters}},\ \ \underbrace{\frac{T_1}{\sigma_Y},\ \ \frac{T_S}{T_1},\ \ \frac{G_{1C}}{\sigma_Y l},\ \ \frac{G_{SC}}{G_{1C}},\ \ \frac{\bar{K}_n}{\sigma_Y},\ \ \frac{\bar{K}_S}{\sigma_Y}}_{\text{interfacial parameters}}\right) \tag{13}$$

Especially, since the mixed-mode cohesive interface model is adopted for a mixed-mode loading case, there exist two additional important parameters (T_S/T_1 and G_{SC}/G_{1C}) compared to conventional cohesive interface model. Intragranular parameters are Young's modulus E, Poisson's ratio v, strain hardening exponent N and grain size d, respectively. The interfacial parameters of grain boundary are maximum separation strengths T_1 and T_S, mode I and shear mode critical fracture energy release rates G_{1C} and G_{SC}, effective initial separation modulus $\bar{K}_n = K_n l = T_1/(\delta_n^0/l)$ and $\bar{K}_S = K_S l = T_S/(\delta_s^0/l)$, respectively.

For convenience, we define a mixed angle of the limit traction ratio of pure shear mode with pure separation mode as

$$\varphi = \arctan(T_S/T_1) * 180/\pi \tag{14}$$

where $\varphi = 90^\circ$ and $\varphi = 0^\circ$ correspond to the shearing separation case and normal separation case, respectively. Similarly, another mixed angle of the limit energy release rate ratio of pure shear mode with pure separation mode can be defined as

$$\Phi = \arctan(G_{SC}/G_{1C}) * 180/\pi \tag{15}$$

where $\Phi = 90^\circ$ and $\Phi = 0^\circ$ correspond to the tangential separation case and normal separation case, respectively. So, the function of stress with strain and several normalized independent parameters (equation (13)) can be rewritten as follows:

$$\frac{\sigma}{\sigma_Y} = g\left(\varepsilon;\ \underbrace{\frac{E}{\sigma_Y},\ \ v,\ \ N,\ \ \frac{d}{l}}_{\text{intragranular parameters}},\ \ \underbrace{\frac{T_1}{\sigma_Y},\ \ \varphi,\ \ \frac{G_{1C}}{\sigma_Y l},\ \ \Phi,\ \ \frac{\bar{K}_n}{\sigma_Y},\ \ \frac{\bar{K}_S}{\sigma_Y}}_{\text{interfacial parameters}}\right) \tag{16}$$

Referring to equation (9), generally, the relative separation displacement δ_m is also a function of the strain and several normalized independent parameters (see equation (16)), so damage variable D can be expressed as follows:

$$D = \begin{cases} 0, & \delta_m \le \delta_m^0 \\ \dfrac{\delta_m^f(\delta_m - \delta_m^0)}{\delta_m(\delta_m^f - \delta_m^0)} = \Psi\left(\varepsilon;\ \dfrac{E}{\sigma_Y},\ v,\ N,\ \dfrac{d}{l},\ \dfrac{T_1}{\sigma_Y},\ \varphi,\ \dfrac{G_{1C}}{\sigma_Y l},\ \Phi,\ \dfrac{\bar{K}_n}{\sigma_Y},\ \dfrac{\bar{K}_S}{\sigma_Y}\right), & \delta_m^0 < \delta_m \le \delta_m^f \\ 1, & \delta_m \ge \delta_m^f \end{cases} \tag{17}$$

According to the definition of damage valuable D from the cohesive interface model (equations (9) and (17)), the variation of D with grain boundary deformation will closely be dependent on the grain boundary directions. For example, the NC material consisting of the hexagonal grains underwent the tension along the vertical direction as shown in Figure 5. There are two kinds of grain boundaries, inclined grain boundary and horizontal grain boundary, corresponding to two representative cohesive elements 1 and 2, respectively, and corresponding to the interface fracture path, as shown in Figure 5. So, in the present research, we shall investigate the overall stress–strain relations of the NC material accompanied by these two kinds of interface damage evolutions which are described by two cohesive elements, respectively.

Overall stress–strain relation and damage evolution relation (equations (16) and (17)) can be calculated in the present research by using the finite element simulations.

FEM

FEM is used in numerical simulations for overall mechanical behavior of NC material. Generally speaking, when the strain gradient effect is considered, the conventional FEM fails (Wei, 2006). Fortunately, the CMSG theory is a lower order strain gradient theory without involving the higher order stress. In this case, the governing equation, boundary conditions and algorithms usually employed in classical mechanics are readily available and can be conveniently applied to study problem when strain gradient effect is considered. One can easily modify the existing finite element program to incorporate the plastic strain gradient effect approximately (Swaddiwudhipong et al., 2006). In the present research, we have implemented a C^0 three-dimensional solid element incorporating the CMSG theory in the ABAQUS software via its user subroutine UMAT.

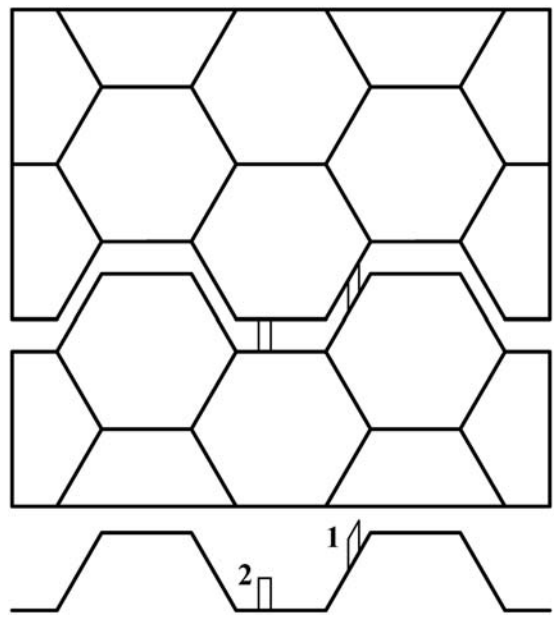

Figure 5. Illustration of two kinds of grain boundary damage features, along the horizontal and inclined grain boundaries.

The influences of intragranular and interfacial parameters on the overall mechanical behaviors are investigated by using the FEM. The study is based on a reference parameters selected by the comparison results between present model and the experimental measurements (in Results and Discussions section). The reference parameters used in the present research are selected as (otherwise it is specified): $E/\sigma_Y = 166.6$, $\nu = 0.3$, $N = 0.2$, $T_S = T_I = \sigma_Y$, $G_{SC} = G_{IC} = 0.053\sigma_Y l$, $l = l_0 = 18\alpha^2(\mu/\sigma_Y)^2 b \approx 1\mu m$ (Huang et al., 2004), where $b = 0.2\,nm$ is magnitude of Burgers vector; and α is an empirical coefficient around 0.3. In the parametric study of present research, $\bar{K}_n$ and $\bar{K}_S$ is taken as Young's modulus of crystal grain.

The finite element mesh adopted in the present research is shown in Figure 6. The grain interior is discredited with hexahedron, eight-node continuum elements C3D8, while the cohesive elements with zero thickness used to simulate grain boundaries are hexahedron, eight-node cohesive elements COH3D8. The element numbers of both C3D8 and COH3D8 for a cell model are 3883 and 342, respectively.

Results and discussions

Considering the NC material cell consisting of the hexagonal grains under uniform tension in vertical direction, the overall stress–strain relations and damage evolutions are analyzed.

As shown in Figure 3, considering the cell with the periodic boundary conditions under unidirectional tension (in y), vertical normal stress σ_{22}/σ_Y is calculated first, and the stress cloud figure is

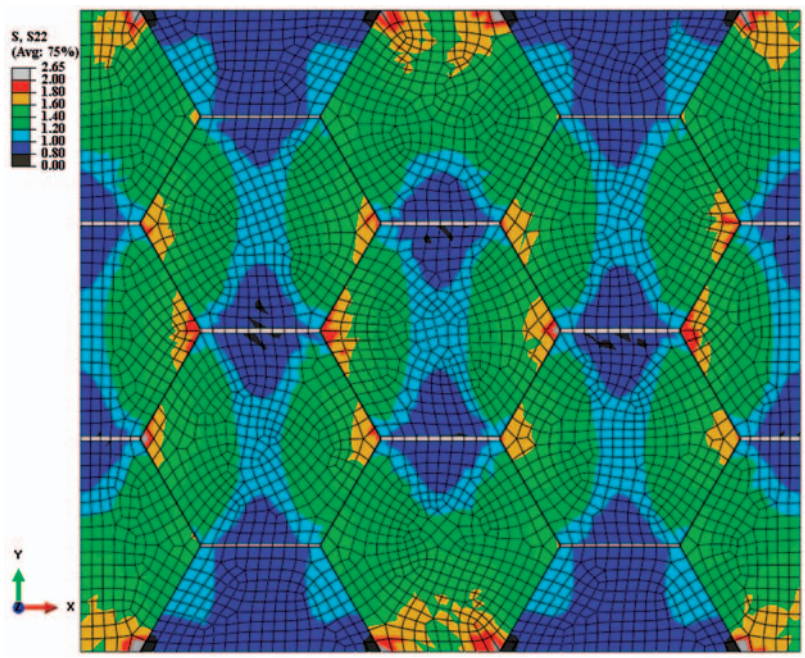

Figure 6. Cloud figure of the normalized stress σ_{22}/σ_Y (loading direction is along y direction) is shown for $d = 0.1l_0$, $\Phi = 45^\circ$. Its average value corresponds to overall stress and the peak stress when exerting load reaches maximum value. $E/\sigma_Y = 166.6$, $\nu = 0.3$, $N = 0.2$, $T_S = T_I = \sigma_Y$, $l_0 = 1\mu m$, $G_{SC} = G_{IC} = 0.053\sigma_Y l_0$.

given in Figure 6. Average value of the vertical normal stress is the ''overall stress'' of cell material, and its limit value is called the ''peak stress'' in the present research. From the distribution of vertical normal stress in Figure 6, clearly, there exist three-level loading regions, described by yellow, green and blue colors. The yellow (or red) color region is the high-stress region, while the blue color region is the low-stress region.

Figures 7 and 8 show the overall stress–strain relations and corresponding damage evolution curves of grain boundary, respectively, for two extreme cases of separation strengths ($T_1/\sigma_Y = 0.5,6.0$). From figures, the overall stress–strain relations can be divided into three stages (I, II and III), which correspond to elastic, hardening and softening stages, respectively. For the case of $T_1/\sigma_Y = 0.5$, the stage I covers the range $0 \leq \sigma/\sigma_Y \leq (T_1/\sigma_Y) = 0.5$, and the horizontal boundary has been in damage state before the initial yield occurs in grain interiors. For the case of $T_1/\sigma_Y = 6.0$, the stage I covers the range $0 \leq \sigma/\sigma_Y \leq 1.0$. Until the grain reaches its initial yield and gets into the yield, the overall stress–strain relation enters the elastic–plastic deformation stage (II).

For the case of $T_1/\sigma_Y = 0.5$, in the stage II the damage initiates and evolutes along the horizontal grain boundary. To the end of stage II (at peak stress point), the damage initiates on the inclined grain boundary. After the peak stress point, the stress–strain curve enters the stage III and damage evolutes along both horizontal and inclined grain boundaries until grain boundary fracture.

For the case of $T_1/\sigma_Y = 6$, since the grain boundary strength is very high, before the stage II the grain boundary damage does not occur. Then, when overall stress reaches the peak stress ($\sigma/\sigma_Y \approx 4.7$, the end of the stage II), the damage initiates from the horizontal grain boundary. The stage III is a very short process and the overall strength of the NC material is lost very quickly accompanied by the damage evolution along the horizontal and inclined grain boundaries.

In Figure 7, the stage II range is smaller than that of stage III, while the case is opposite for Figure 8. The stage II mainly represents the intragranular deformation while the stage III mainly describes damage evolution along the grain boundaries. Therefore, when $T_1 < \sigma_Y$, the overall strength and ductility of the NC material are mainly dominated by the grain boundary damage

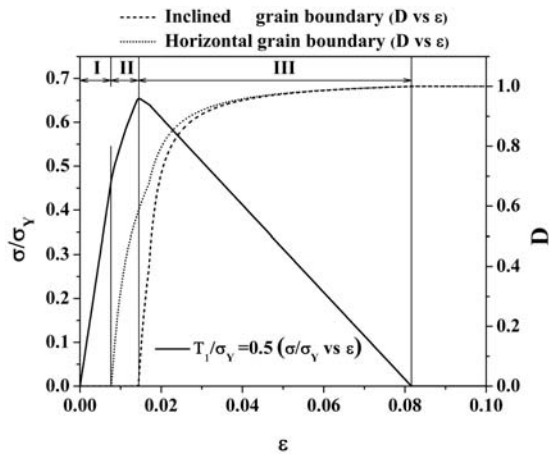

Figure 7. Overall stress–strain relation and damage evolution relation for $T_1/\sigma_Y = 0.5$ and $d = 0.1l_0$. $E/\sigma_Y = 166.6$, $\nu = 0.3$, $N = 0.2$, $l_0 = 1\mu m$, $G_{SC} = G_{IC} = 0.053\sigma_Y l_0$.

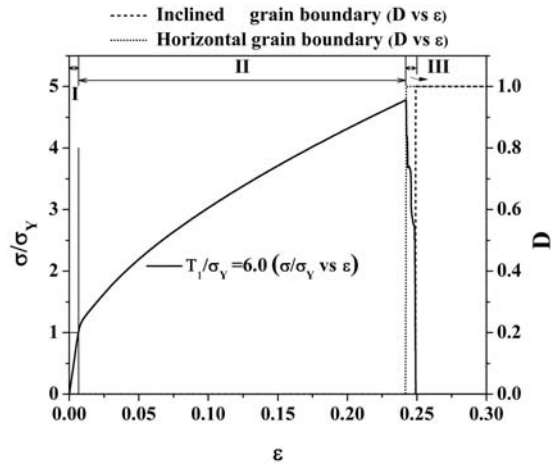

Figure 8. Overall stress–strain relation and damage evolution relation for $T_1/\sigma_Y = 6.0$ and $d = 0.1l_0$. $E/\sigma_Y = 166.6$, $\nu = 0.3$, $N = 0.2$, $l_0 = 1\mu m$, $G_{SC} = G_{1C} = 0.053\sigma_Y l_0$.

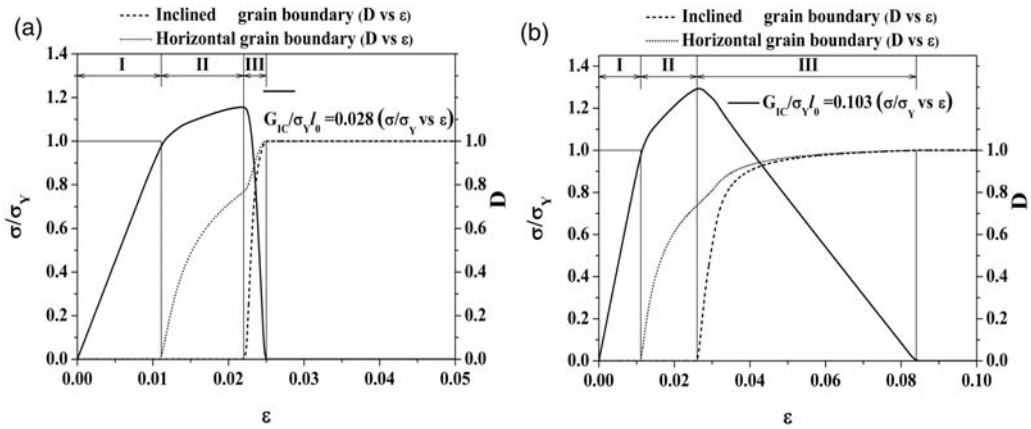

Figure 9. Overall stress–strain relations and damage evolution relations: $E/\sigma_Y = 166.6$, $\nu = 0.3$, $N = 0.2$, $T_S = T_1 = \sigma_Y$, $l_0 = 1\mu m$ (a) for $G_{1C}/\sigma_Y l_0 = 0.028$ and $d = 0.1l_0$; (b) for $G_{1C}/\sigma_Y l_0 = 0.103$ and $d = 0.1l_0$.

evolution, while when $T_1 > \sigma_Y$, they are mainly dominated by the intragranular elastic–plastic behaviors.

Figure 9(a) and (b) show the overall stress–strain curves and the corresponding damage evolution curves, respectively, for $G_{1C}/\sigma_Y l_0 = 0.028$ and 0.103. The results illustrate that the overall stress–strain curves can also be divided into three stages (I, II and III). The interpretations of three stages are same as those in Figures 7 and 8. The most obvious difference here is the range of stage III (damage evolutions cause grain boundary fracture). For the case of $G_{1C}/\sigma_Y l_0 = 0.103$, the range of stage III is much larger than that of the case of $G_{1C}/\sigma_Y l_0 = 0.028$. So, the parameter G_{1C} (critical grain boundary energy release rate) is an important parameter that controls the ductility of the NC materials.

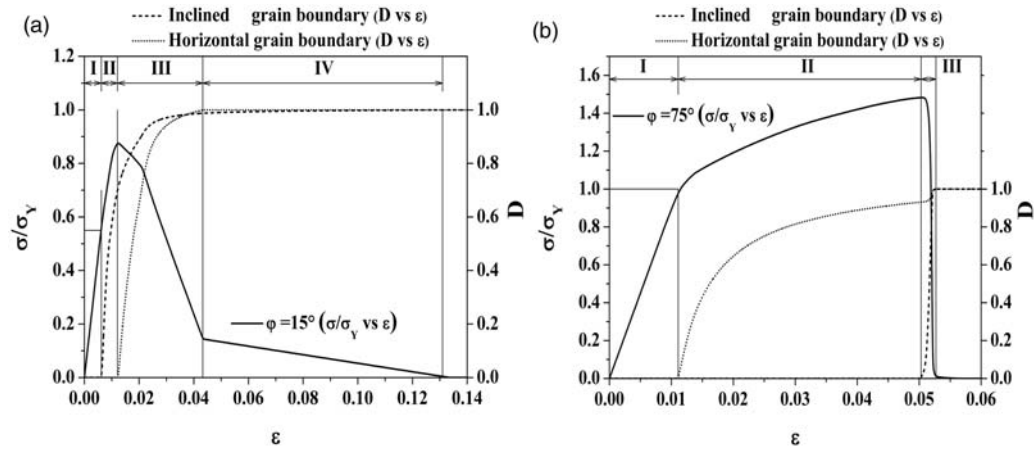

Figure 10. Overall stress–strain relations and damage evolution relations: $E/\sigma_Y = 166.6$, $\nu = 0.3$, $N = 0.2$, $T_1 = \sigma_Y$, $l_0 = 1\mu m$, $G_{SC} = G_{1C} = 0.053\sigma_Y l_0$ (a) for $\varphi = 15^\circ$, $d = 0.1l_0$ (b) for $\varphi = 75^\circ$, $d = 0.1l_0$.

Figure 10(a) and (b) show the overall stress–strain curves and the corresponding damage evolution curves, respectively, for $\varphi = 15^\circ, 75^\circ$ and $d = 0.1l_0$. For the case of $\varphi = 15^\circ$ (referring to equation (14) for its definition), the overall stress–strain curves can be divided into four stages (I, II, III and IV), while for $\varphi = 75^\circ$, it corresponds to three stages (I, II and III). For the case of $\varphi = 15^\circ$, since T_S is less than T_1, the damage initiation and evolution along the inclined grain boundary occur first in the stage II, and they develop quickly along both horizontal and inclined grain boundaries in two stages (III and IV). For the case of $\varphi = 75^\circ$, since T_1 is less than T_S, the damage initiation and evolution along the horizontal grain boundary are easy during the stage II, until the end of stage II the damage initiation occurs along the inclined grain boundary.

Comparing the ranges of stage II in Figure 10(a) and (b) indicates that the intragranular elastic–plastic deformation plays an important role in the overall strength and ductility of the NC material with increasing φ. T_S/T_1 is also a critical control parameter for the competition of grain boundary deformation with that in the grain interiors to define the global strength and ductility of the NC material.

Figure 11(a) to (c) show the overall stress–strain curves and corresponding damage evolution curves, respectively, for $\Phi = 15^\circ, 45^\circ, 75^\circ$ and $d = 0.1l_0$. For the cases of $\Phi = 15^\circ, 75^\circ$(referring to equation (15) for its definition), the overall stress–strain curves can be divided into four stages (I, II, III and IV), while it is divided into three stages for the case of $\Phi = 45^\circ$. On comparing Figure 11(a) with 11(c), one can find that to the end points of the stage III, for case $\Phi = 15^\circ$, the inclined grain boundary first enters the full damage state ($D = 1$), while for case $\Phi = 75^\circ$, the horizontal grain boundary first enters the full damage state. From the results shown in the Figure 11(a)–(c), we can find that the parameter G_{SC}/G_{1C} is important to govern the ductility of the NC material.

The overall strength and ductility of the NC material can be described by the peak stress and failure strain, which have been shown in the results of above Figures 7–11.

From Figures 7–11, cohesive interface models are used to describe the damage and fracture process of the grain boundaries of the NC materials, so that the shapes of the overall stress–strain relations obtained closely reflect the grain boundary's damage process.

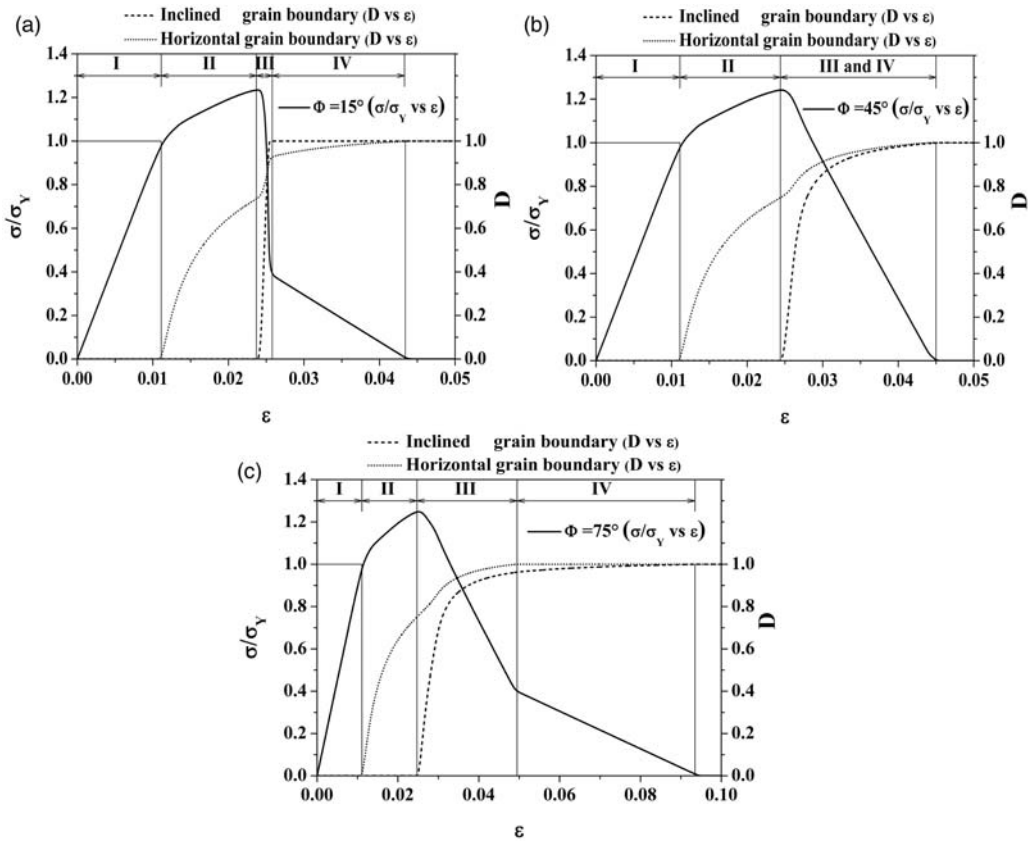

Figure 11. Overall stress–strain relations and damage evolution relations: $E/\sigma_Y = 166.6$, $\nu = 0.3$, $N = 0.2$, $T_S = T_I = \sigma_Y$, $l_0 = 1\mu m$, $G_{IC} = 0.053\sigma_Y l_0$ (a) for $\Phi = 15^\circ$, $d = 0.1l_0$; (b) for $\Phi = 45^\circ$, $d = 0.1l_0$; (c) for $\Phi = 75^\circ$, $d = 0.1l_0$.

Besides the parameters depended as discussed above, both the peak stress and the failure strain have the dependences on the other parameters, such as the Young's modulus, strain hardening exponent, as well as the grain size. Figure 12(a) and (b) show the variations of both peak stress and failure strain with Young's modulus for three grain size cases $d = 0.1l_0$, $1.0l_0$ and $10l_0$, respectively. From Figure 12(a) and (b), the peak stresses of the NC material slowly increase with increasing the intragranular elastic modulus, while the failure strains (describing the overall ductility) slowly decrease with increasing Young's modulus. Figure 13(a) and (b) show the variations of both peak stress and failure strain with strain hardening exponent for three grain size cases $d = 0.1l_0$, $1.0l_0$ and $10l_0$, respectively. From Figure 13(a) and (b), the trend of influence of N on the peak stresses and the failure strains (describing the overall ductility of the NC material) is the same as that of Young's modulus E.

In order to verify the validity of the present model, we use our model to simulate some cases where the experimental investigations were performed. The first experiment is on the NC Cu under uniaxial tension was reported in Sanders et al. (1997), and the second experiment on NC Ni uniaxial tension was reported in Zhu et al. (2005).

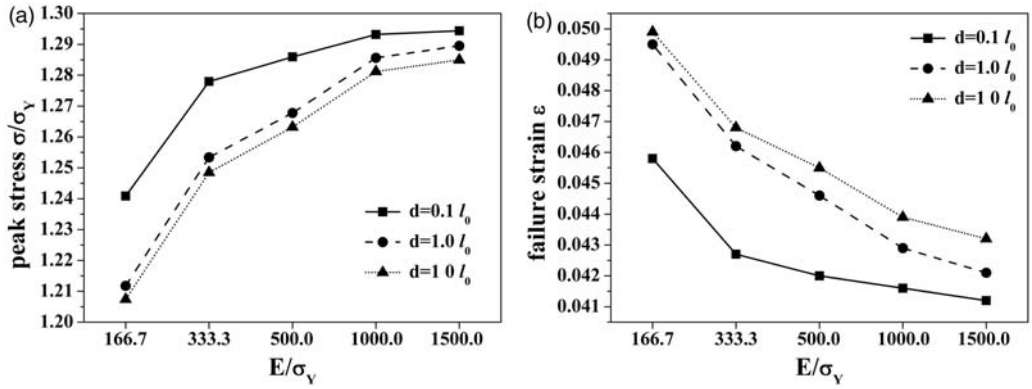

Figure 12. (a) The dependence of the strength (peak stress) on elastic modulus (E/σ_Y) of grain Interior for three grain sizes. (b) The dependence of the ductility (failure strain) on elastic modulus (E/σ_Y) of grain interior for three grain sizes. $\nu = 0.3$, $N = 0.2$, $T_S = T_1 = \sigma_Y$, $l_0 = 1\mu m$, $G_{SC} = G_{1C} = 0.053\sigma_Y l_0$.

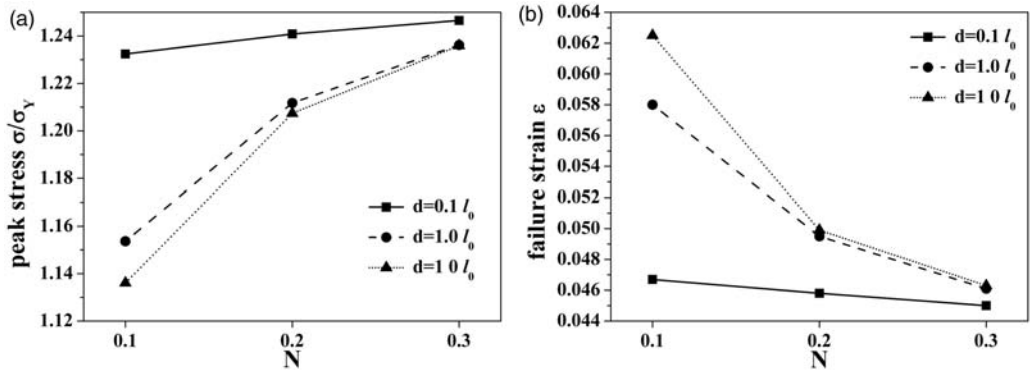

Figure 13. (a) The dependence of the strength (peak stress) on strain hardening exponent (N) of grain interior for three grain sizes. (b) The dependence of the ductility (failure strain) on strain hardening exponent (N) of grain interior for three grain sizes. $E/\sigma_Y = 166.6$, $\nu = 0.3$, $T_S = T_1 = \sigma_Y$, $l_0 = 1\mu m$, $G_{SC} = G_{1C} = 0.053\sigma_Y l_0$.

In our simulation, the parameters of grain interior and the grain boundary for NC Cu and NC Ni are listed in Tables 1 and 2, respectively.

The grain boundary strength parameter T_1 is chosen to coincide with the yield strength σ_Y, while grain boundary parameter T_S is generally selected in the range from yield strength σ_Y to shear strength for fcc metals, which is usually estimated as $\mu/30$ (μ is the shear modulus) (Wei and Anand, 2004). For normal separation case such as in Wu and Wei (2010), one needs to consider only T_1, without T_S, but for the present mixed mode we need to consider effect from both T_S (or T_1) and T_S/T_1.

Figure 14(a) and (b) show the comparisons between our model results and the corresponding experimental data for NC Cu and NC Ni, respectively. From figures, the predicted stress–strain curves maintain a good agreement with the experimental data under tension.

Table 1. Simulation parameters for grain of nanocrystalline metals, Cu and Ni (Sanders et al. (1997) and Zhu et al. (2005)).

Nc metal	E (GPa)	v	b (nm)	d (nm)	σ_Y (GPa)
Cu	134	0.35	0.25	49	0.24
Ni	210	0.3	0.3	20	1.2

Table 2. Simulation parameters for mixed-mode cohesive interface of nanocrystalline metals, Cu and Ni.

Nc metal	T_I (GPa)	T_S (GPa)	G_{IC} (J/m^2)	G_{SC} (J/m^2)
Cu	0.24	1.5	80	80
Ni	1.2	1.5	30	30

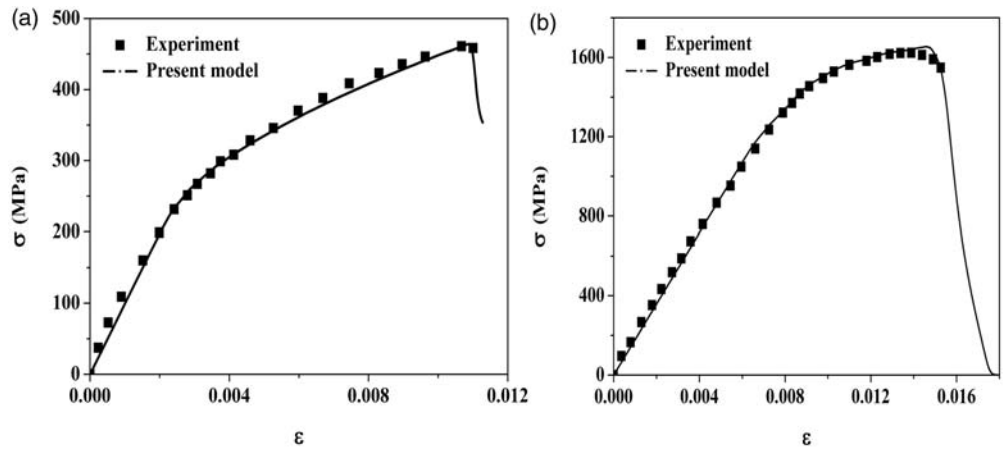

Figure 14. Comparison of results (overall stress strain relation) between present model and the experimental data for nanocrystalline metals (a) for NC Cu and (b) for NC Ni.

The present simulations for the experiments confirm that the present model and FEM method developed for the NC materials are effective. The model and the numerical method can be used to describe the mechanical behavior of NC metals effectively.

Conclusions

In the present investigation, overall mechanical behaviors of the NC materials considering the grain boundary damage evolutions have been investigated systematically. The mixed-mode cohesive interface model has been used to describe the mixed deformation and fracture process of grain boundaries. Based on the mixed-mode cohesive interface model, the grain boundary damage and damage evolution have been defined and characterized. The strain gradient plasticity theory has been used to describe the grain materials and grain size effect. In the present results, the overall stress–strain

relations and corresponding damage evolution curves have been computed and obtained as functions of several major parameters of materials and grain boundaries, such as the normalized separation strength T_1/σ_Y, critical separation energy release rate $G_{1C}/\sigma_Y l$, strength mixity T_S/T_1, energy release rate mixity G_{SC}/G_{1C}, Young's modulus and strain hardening exponent. From the modeling and simulation results, we have found that the grain boundary properties play the critical role in the overall mechanical behaviors of the NC materials, and the grain boundary damage evolution dominates the shape of the overall stress–strain relations. By using the damage evolution relations, we have made a clear interpretation on the features of the overall stress–strain curves.

Funding

This work was supported by National Basic Research Program of China through 2012CB937500 and by the National Natural Science Foundation of China through grants 11021262, 10932011 and 91116003.

Acknowledgement

Li Chen would like to thank Dr Wei Xu, Institute of Mechanics, Chinese Academy of Sciences, for his helpful advice.

References

Barenblatt GI (1959) The formation of equilibrium cracks during brittle fracture. General ideas and hypothesis. Axially-symmetric cracks. *Prikladnaya Matematika i Mekhanika* 23: 434–444.

Barenblatt GI (1962) Mathematical theory of equilibrium cracks in brittle fracture. *Advances in Applied Mechanics* 7: 55–125.

Cao A and Wei Y (2007) Atomistic simulations of crack nucleation and intergranular fracture in bulk nanocrystalline nickel. *Physical Review B* 76: 024113.

Dugdale DS (1960) Yielding of steel sheets containing slits. *Journal of the Mechanics and Physics of Solids* 8: 100–104.

Evans AG and Hutchinson JW (2009) A critical assessment of theories of strain gradient plasticity. *Acta Materialia* 57: 1675–1688.

Fu HH, Benson DJ and Meyers MA (2004) Computational description of nanocrystalline deformation based on crystal plasticity. *Acta Materialia* 52: 4413–4425.

Gao H, Huang Y, Nix WD, et al (1999) Mechanism-based strain gradient plasticity – I. Theory. *Journal of the Mechanics and Physics of Solids* 47: 1239–1263.

Gleiter H (2000) Nanostructured materials: Basic concepts and microstructure. *Acta Materialia* 48: 1–29.

Hasnaoui A, Van Swygenhoven H and Derlet PM (2003) Dimples on nanocrystalline fracture surfaces as evidence for shear plane formation. *Science* 300: 1550–1552.

Huang Y, Qu S, Hwang KC, et al (2004) A conventional theory of mechanism-based strain gradient plasticity. *International Journal of Plasticity* 20: 753–782.

Hutchinson JW (1976) Bounds and self-consistent estimates for creep of polycrystalline materials. *Proceedings of the Royal Society of London A* 348: 101–127.

Kok S, Beaudoin AJ and Tortorelli DA (2002) A polycrystal plasticity model based on the mechanical threshold. *International Journal of Plasticity* 18: 715–741.

Kumar KS, Van Swygenhoven H and Suresh S (2003) Mechanical behavior of nanocrystalline metals and alloys. *Acta Materialia* 51: 5743–5774.

Mi Y, Crisfield MA, Davies GAO, et al (1998) Progressive delamination using interface elements. *Journal of Composite Materials* 32: 1246–1272.

Needleman A (1990) An analysis of tensile decohesion along an interface. *Journal of the Mechanics and Physics of Solids* 38: 289–324.

Nilsson K and Lidstrom P (2012) Simulation of ductile fracture of slabs subjected to dynamic loading using cohesive elements. *International Journal of Damage Mechanics* 21: 871–892.

Omiya M and Kishimoto K (2010) Damage-based cohesive zone model for rate-depend interfacial fracture. *International Journal of Damage Mechanics* 19: 397–420.

Ovid'ko IA (2007) Review on the fracture processes in nanocrystalline materials. *Journal of Materials Science* 42: 1694–1708.

Sanders PG, Eastman JA and Weertman JR (1997) Elastic and tensile behavior of nanocrystalline copper and palladium. *Acta Materialia* 45: 4019–4025.

Schiotz J, Vegge T, Di Tolla FD, et al (1999) Atomic-scale simulations of the mechanical deformation of nanocrystalline metals. *Physical Review B* 60: 11971–11983.

Schwaiger R, Moser B, Dao M, et al (2003) Some critical experiments on the strain-rate sensitivity of nanocrystalline nickel. *Acta Materialia* 51: 5159–5172.

Shan ZW, Stach EA, Wiezorek JMK, et al (2004) Grain boundary-mediated plasticity in nanocrystalline nickel. *Science* 305: 654–657.

Swaddiwudhipong S, Tho KK, Hua J, et al (2006) Mechanism-based strain gradient plasticity in C-0 axisymmetric element. *International Journal of Solids and Structures* 43: 1117–1130.

Truong DV and Kitamura T (2010) Cohesive zone model applied to creep crack initiation at an interface edge between submicron thick films. *International Journal of Damage Mechanics* 19: 301–319.

Turon A, Camanho P, Costa J, et al. (2004) An interface damage model for the simulation of delamination under variable-mode ratio in composite materials. *NASA/TM-2004-213277*.

Tvergaard V and Hutchinson JW (1992) The relation between crack growth resistance and fracture process parameters in elastic–plastic solids. *Journal of the Mechanics and Physics of Solids* 40: 1377–1397.

Van der Sluis O, Schreurs PJG and Meijer HEH (2001) Homogenisation of structured elastoviscoplastic solids at finite strains. *Mechanics of Materials* 33: 499–522.

Van Swygenhoven H and Derlet PA (2001) Grain-boundary sliding in nanocrystalline fcc metals. *Physical Review B* 64: 224105.

Van Vliet KJ, Tsikata S and Suresh S (2003) Model experiments for direct visualization of grain boundary deformation in nanocrystalline metals. *Applied Physics Letters* 83: 1441–1443.

Warner DH, Sansoz F and Molinari JF (2006) Atomistic based continuum investigation of plastic deformation in nanocrystalline copper. *International Journal of Plasticity* 22: 754–774.

Wei Y (2006) A new finite element method for strain gradient theories and applications to fracture analyses. *European Journal of Mechanics A – Solids* 25: 897–913.

Wei Y, Chen X, Shu S, et al (2006) Nonuniformity effect of surface-nanocrystalline materials in nanoindentation test. *International Journal for Multiscale Computational Engineering* 4: 183–195.

Wei YG and Hutchinson JW (1997a) Steady-state crack growth and work of fracture for solids characterized by strain gradient plasticity. *Journal of the Mechanics and Physics of Solids* 45: 1253–1273.

Wei YG and Hutchinson JW (1997b) Nonlinear delamination mechanics for thin films. *Journal of the Mechanics and Physics of Solids* 45: 1137–1159.

Wei YG, Shu SQ, Du Y, et al (2005) Size, geometry and nonuniformity effects of surface-nanocrystalline aluminum in nanoindentation test. *International Journal of Plasticity* 21: 2089–2106.

Wei YJ and Anand L (2004) Grain-boundary sliding and separation in polycrystalline metals: Application to nanocrystalline fcc metals. *Journal of the Mechanics and Physics of Solids* 52: 2587–2616.

Wu B, Liang LH, Ma HS, et al (2012) A trans-scale model for size effects and intergranular fracture in nanocrystalline and ultra-fine polycrystalline metals. *Computational Materials Science* 57: 2–7.

Wu B and Wei YG (2010) A computational model for intergranular fracture in nanocrystalline and ultra-fine polycrystalline metals. *Materials Science Forum* 633–634: 39–53.

Xu W, Lu TJ and Wang F (2010) Effects of interfacial properties on the ductility of polymer-supported metal films for flexible electronics. *International Journal of Solids and Structures* 47: 1830–1837.

Zhu B, Asaro RJ, Krysl P, et al (2005) Transition of deformation mechanisms and its connection to grain size distribution in nanocrystalline metals. *Acta Materialia* 53: 4825–4838.